New Journal of Physics
The open access journal for physics

Time-and-energy-resolved measurement of Auger cascades following Kr 3d excitation by attosecond pulses

A J Verhoef[1,8], A V Mitrofanov[1], X T Nguyen[1], M Krikunova[2,3], S Fritzsche[4,5], N M Kabachnik[6,7], M Drescher[2] and A Baltuška[1]

[1] Institut für Photonik, Technische Universität Wien, Gusshausstrasse 27-29/387, 1040 Wien, Austria
[2] Institut für Experimentalphysik, Universität Hamburg, Luruper Chaussee 149, 22761 Hamburg, Germany
[3] Institut für Optik und Atomare Physik, Technische Universität Berlin, Hardenbergstrasse 36, 10623 Berlin, Germany
[4] Atomic Physics Division, GSI Helmholtzzentrum für Schwerionenforschung, Planckstrasse 1, 64291 Darmstadt, Germany
[5] Department of Physics, University of Oulu, Post Office Box 3000, Fin-90014 Oulu, Finland
[6] Institute of Nuclear Physics, MV Lomonosov Moscow State University, Vorobyevy gory, Moscow 119991, Russia
[7] European XFEL GmbH, Albert-Einstein-Ring 19, 22761 Hamburg, Germany
E-mail: averhoef@mail.tuwien.ac.at

New Journal of Physics **13** (2011) 113003 (19pp)
Received 4 September 2011
Published 3 November 2011
Online at http://www.njp.org/
doi:10.1088/1367-2630/13/11/113003

Abstract. We show that attosecond metrology has evolved from proof-of-principle experiments to a level where complex processes can be resolved in time that cannot be accessed using any other existing technique. The cascaded Auger decay following ionization and excitation of the 3d-subshell in Kr with subfemtosecond 94 eV soft x-ray pulses has been energy- and time-resolved in an x-ray pump–infrared probe experiment. This Auger cascade reveals rich multi-electron dynamics, which despite the fact that there are many experimental and theoretical data available, is not yet fully understood. We present time-resolved data showing the sequence of the temporal dynamics in the cascaded Auger

[8] Author to whom any correspondence should be addressed.

decay. The decay time of several groups of lines has been measured, including the lines at the low-energy part of the spectrum, which are predominantly produced by the second-step Auger transitions. Our experimental data reveal long lifetimes (up to 70 fs) of the subvalence excited ionic (intermediate) states in the cascaded resonant Auger decay. Extensive theoretical calculations within the multiconfiguration Dirac–Fock (MCDF) approach show that the observed long lifetime may be attributed to the second-step Auger decay of the resonantly excited $3d^{-1}np$ states with $n = 6, 7$. Furthermore, our experimental data show that the electrons with a kinetic energy around 25 eV (generally assigned as $M_{4,5}N_1N_1\,{}^1S_0$ normal Auger lines) have a component corresponding to the second-step Auger decay of the ion after resonant Auger transition $3d^{-1}np \rightarrow 4s^2\,4p^3\,4dnp \rightarrow 4s^2\,4p^4$ with a lifetime of 26 ± 4 fs.

Contents

1. Introduction

Absorption of energetic photons can create highly excited atoms or ions, since the high-energy photons couple more effectively to core electrons than to the valence electrons. The highly excited state decays very quickly, through different channels, both radiative and non-radiative. In light and medium-sized atoms the dominant relaxation channel is non-radiative (Auger) decay where in one or more decay steps one or more electrons are emitted. The Auger decay provides insight into the interaction of electrons in the atom or ion, which is of key importance for the understanding of many-electron systems. A great deal of information about the Auger process in atoms has been accumulated by means of steady-state electron and ion spectroscopy in ionization of atoms by synchrotron radiation in the extreme ultraviolet (XUV) and soft x-ray energy range (see, e.g., [1] and references therein). Modern high-resolution electron spectroscopy allows one to measure the width of Auger lines with high precision and thus obtain information about the Auger decay time [2]. Similarly, Auger cascades have been studied by steady-state measurements (see [3] and references therein).

Progress in attosecond physics has led to the appearance of new, time-resolved methods of investigation of Auger decay. In pioneering experiments [4, 5], the Auger process was started by a subfemtosecond XUV pulse and probed by a few-femtosecond infrared (IR) laser pulse, providing direct information about the time development of the Auger decay. Recent advances in attosecond pump–probe ion-charge-state spectroscopy [6, 7] have extended the time-resolved methods to the study of Auger cascades. In these experiments, information about the time

constants at various steps of the Auger cascade has been gained, which could not be obtained by steady-state spectroscopic methods. However, in contrast to kinetic-energy resolved electron detection, the photo-ion detection used in [6, 7] does not allow one to unambiguously determine the intermediate levels involved in the cascade and thus provides only integral information averaged over many transitions.

In this paper, we use an electron time-of-flight spectrometer to measure the electron spectra in an XUV pump–IR probe time-resolved experiment, similar to [4], in order to investigate the individual pathways of the cascaded Auger decay and to study their time evolution. In the experiment krypton atoms are photoexcited in the 3d shell by subfemtosecond XUV pulses with a central energy of 94.4 eV. The choice of krypton as a target is connected with the fact that both normal Auger decay and resonant Auger decay of Kr(3d) are very well studied in the literature by means of electron spectroscopy at synchrotron radiation facilities [2, 8–16]. The spectra, the lifetimes of the initial excited states and even the angular distributions of Auger electrons have been investigated with high accuracy. The spectra of the cascaded Auger electrons and their angular distributions have also been measured [11, 15, 17]. On the other hand, the cited experiments could not give information about the time evolution of the cascade. Such information can be obtained only by time-resolved measurements.

In figure 1, which is based on [7] but with the $4\,s^{-2}$ level corrected, the 3d excitation (dash-dotted blue arrows) of krypton by an attosecond XUV pulse and the subsequent Auger decay (both resonant—dashed magenta arrows—and normal—solid red arrows) are schematically shown. The further cascaded Auger decay is indicated with short-dashed green arrows. Since the attosecond XUV pulse has a large bandwidth of about 6 eV (full-width at half-maximum (FWHM)), both normal and resonant Auger transitions are induced. As can be seen from figure 1, triply charged Kr ions can be produced either directly or after a cascaded Auger decay from singly 3d core-ionized atoms. Doubly charged krypton ions can be produced directly, after a cascaded Auger decay from resonantly core-excited Kr, or after a single Auger decay from singly core-ionized Kr. There are many pathways leading to the formation of Kr^{2+} and Kr^{3+} ions, and just by studying the ion yield alone, without measurements of the electron energies, it is not possible to single out a particular cascade.

In our experiment, we observe the electron kinetic energy spectrum as a function of the delay between the XUV pump pulse and the IR probe pulse. When there is a temporal overlap of the probe pulses and the electron emission, either due to direct photoionization or due to Auger emission, the spectrum of the respective features changes due to this overlap. In the case of direct photoionization, spectral broadening and a shift of the central energy of the feature can be observed (attosecond streaking [19]). In the case of the relatively long Auger emission (relaxation time longer than the optical cycle duration), one or more sidebands can be generated, depending on the probe laser intensity.

A preliminary evaluation of the experimental data is presented in the proceedings of the International Laser Physics Workshop 2010 [20]. In this paper we present the complete evaluation of the experimental data, together with the results of extensive numerical calculations that support the experimental findings.

2. Experimental details

The laser system used in the experiment is a 5 kHz Ti:sapphire chirped pulse amplifier (CPA), delivering 0.8 mJ, 25 fs pulses. The output pulses are spectrally broadened in a neon-filled

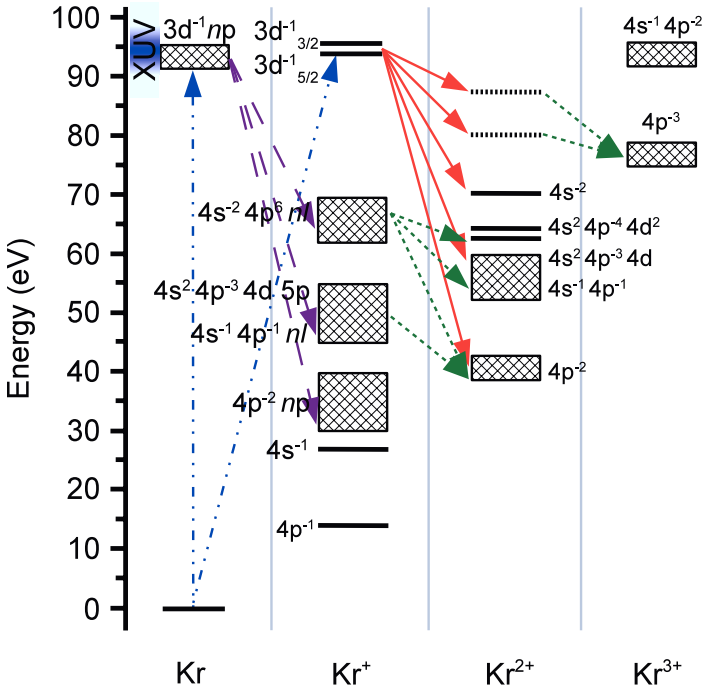

Figure 1. Schematic representation of energy levels and transitions in neutral, singly, doubly and triply ionized krypton. The 3d excitation by the attosecond XUV pulse is depicted by the dash-dotted blue arrows pointing up from the ground state of neutral krypton. The resonant and normal Auger emissions are indicated by the dashed magenta arrows and solid red arrows, respectively. The cascaded Auger emission is indicated with short-dashed green arrows. The scheme is mainly based on [7], with some modifications prompted by [12, 18].

250 μm diameter capillary and subsequently compressed to 5 fs using chirped mirrors (see figure 2). Attosecond XUV pulses are generated by focusing the 250 μJ, 5 fs pulses with a central wavelength of ~750 nm into a neon gas jet, as shown in figure 2. The XUV beam is spatially separated from the IR beam using an annular filter that blocks the IR light and transmits the XUV radiation through a 150 nm zirconium foil in the center, while blocking the XUV radiation and transmitting the IR light on the outside. A focusing two-component annular Mo/Si multilayer mirror is used to induce a tunable delay between the XUV and the IR pulses and to focus the beams on a krypton gas target. The spectral filtering by the zirconium foil transmission and Mo/Si mirror reflectivity of the XUV pulses yields a resulting bandwidth of ~6 eV (FWHM) around 94.4 eV. Streaking measurements of neon 2p electrons allowed us to estimate the pulse duration of the XUV pulses to be ~250 as. The resulting photo-electrons and Auger electrons are analyzed using a time-of-flight electron spectrometer. The delay between the XUV and the IR pulses is controlled with a piezo-actuated delay stage. An active feedback loop ensures a delay accuracy better than 30 as.

The experimentally measured spectra contain Auger lines from both resonantly excited krypton atoms and krypton ions. Thus it is possible to calibrate the time-of-flight spectrometer using the strongest normal Auger lines and the tabulated line positions of [12]. In figure 3 we

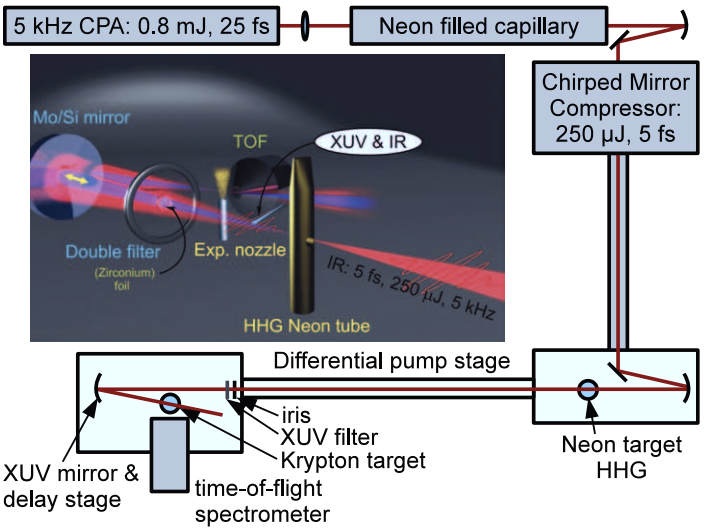

Figure 2. Schematic drawing and rendering of the experimental setup. Attosecond XUV pulses are generated by focusing 250-μJ, 5-fs pulses into a neon gas jet. The XUV pulses are spatially separated from the IR pulses with an annular filter consisting of a 150 nm thin Zr foil at the center and a 2 μm thick pellicle around. A two-component annular Mo/Si multilayer mirror focuses the IR and XUV pulses with a controllable delay onto the krypton target. The IR intensity on the krypton target is controlled with an adjustable iris in front of the annular filter (omitted for clarity in the rendering). The electrons emitted from the krypton jet are analyzed using a time-of-flight spectrometer.

show the measured spectrum at large negative delay (where the IR probe precedes the XUV pump pulse) with bars at the known line positions taken from [9, 10, 12–14]. Using these line positions we fitted the spectrum and obtained the relative line strengths for our experimental conditions. To analyze the spectra at different delays, we combine the lines in several groups, small enough that the sideband formation can be treated jointly, with the condition that it is reasonable to assume that the entire group has the same decay properties (the chosen groups are discussed in more detail in the next section). Each spectrum was then fitted in order to obtain the Auger line and sideband intensities as a function of pump–probe delay. This information can then be analyzed to obtain the decay properties of each group of Auger lines. From the streaking of the emitted Kr 4p electrons we can determine the intensity of the probe pulses in our experiment to be $\sim 5 \times 10^{11}$ W cm^{-2}. A more detailed description of the fitting procedure is provided in the appendix.

In all the fits, we use the raw TOF data, and we do not use the Jacobian correction, i.e. we do not correct for the conversion from the time-of-flight to the energy axis. We do this for several reasons, among the most important ones are: avoiding the need to amplify the statistical noise, the error bars can be computed much more straightforwardly and reliably for the raw data; the throughput of the TOF as a function of kinetic energy is not uniform, i.e. the Jacobian correction would not yield the correct spectrum.

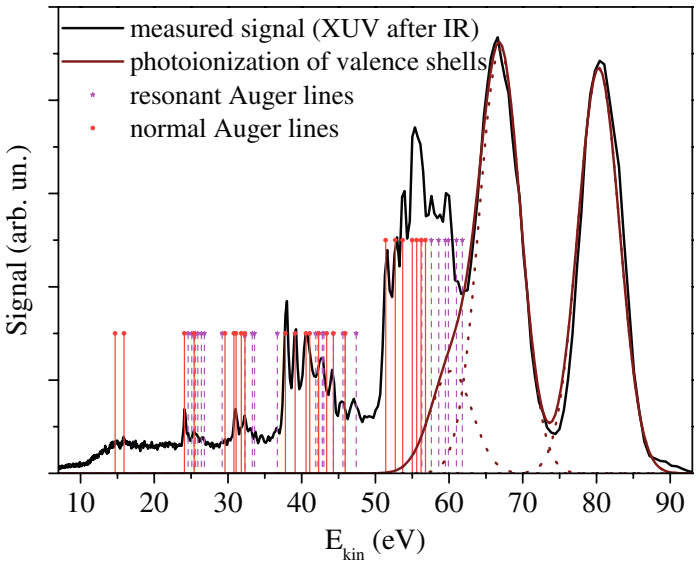

Figure 3. Electron kinetic energy spectrum measured with the IR probe timed well before the XUV pump pulse. At high kinetic energies the photoionization from the valence shells (4s and 4p) is visible (dashed wine-red curves; the solid wine-red curve shows the sum of all relevant valence photoemission features), as well as a shoulder on the 4s peak that can be assigned as the $4p^{-2}5s$ shake-up satellite. The most prominent Auger lines are clearly visible at the positions where they are expected, denoted by vertical red lines and dots (normal Auger) [9, 10, 12] and dashed magenta lines and stars (resonant Auger) [13, 14].

3. Theoretical analysis

In order to support the experiment and to understand the obtained results, we have made extensive calculations of the Auger cascades in Kr, both for the normal Auger transitions from Kr $3d^{-1}$ states and for resonant Auger transitions $3d^{-1}nl$, which are all excited in our experiment. The first-step Auger transitions in Kr(3d) were theoretically studied in [3, 10, 12, 13, 15, 21]. In contrast, the second-step transitions have been investigated much less theoretically. To the best of our knowledge, there is only one published work [15] where the energies and the angular distribution of the second-step Auger electrons in resonant Auger decay from Kr $3d^{-1}5p$ excitations were calculated. Thus, in this paper our main goal is to study the characteristics of the second-step Auger transitions generated by the Kr(3d) excitation.

For the calculations we use the multiconfiguration Dirac–Fock (MCDF) method [22, 23], which has been found to be a versatile tool to calculate wave functions and transition amplitudes of various kinds [24, 25]. In this method, an atomic state with a certain parity π and total angular momentum J is approximated by a linear combination of the so-called configuration state functions (CSF) of the same symmetry

$$|\psi_\alpha(\pi J)\rangle = \sum_{r=1}^{n_c} c_r(\alpha)\,|\gamma_r \pi J\rangle\,, \tag{1}$$

where n_c is the number of CSF and $\{c_r(\alpha)\}$ is the representation of the state in the given many-electron basis. In ansatz (1), moreover, γ_r represents the occupation of the atomic shells as well as all further quantum numbers from the coupling of these shells that are required for a unique specification of the (bound) N-electron basis. In most standard computations, the CSF are constructed as antisymmetrized products of a common set of orthonormal orbitals and are optimized using the Dirac–Coulomb Hamiltonian. The relativistic contributions to the representation $\{c_r(\alpha)\}$ of the atomic states are added by incorporating the Breit interaction into the Hamiltonian matrix [26].

Using the MCDF approach we calculated the energies and wave functions of the atomic states, which are involved in the first- and second-step Auger transitions. As is typical of noble gases, the initial vacancy state $3d^{-1}$ and initial resonant states of the $3d^{-1}np$ excitations are well described within the single (non-relativistic) configuration approximation. In contrast, the intermediate states of Kr^+ and Kr^{2+} already contain in general two or three open shells and, hence, exhibit a strong mixing of nearby configurations. In the present calculations of the normal Auger transitions and the following cascade transitions, 118 intermediate CSF of Kr^{2+} are included with the following non-relativistic configurations: $4s^2\,4p^4$, $4s\,4p^5$, $4s^0\,4p^6$, $4s^2\,4p^3\,4d$, $4s^2\,4p^2\,4d^2$, $4s^2\,4p^3\,5s$ and $4s^2\,4p^3\,5d$, and with $J = 0, 1, 2$ (the levels with $J = 3, 4$ are usually weakly populated and are not considered). The final states of Kr^{3+} are described by mixing 13 CSF of the $4s^2\,4p^3$ and $4s\,4p^4$ configurations. For resonant Auger transitions from Kr $3d^{-1}np$ resonances the calculations have been performed for $n = 5, 6$ and 7, separately. The intermediate states are calculated on the configuration basis of $4s\,4p^5\,np$, $4s^0\,4p^6\,np$, $4s^2\,4p^3\,4d\,np$ and $4s^2\,4p^2\,4d^2\,np$ non-relativistic configurations. For each $n = 5, 6, 7$, these configurations give rise to 496 levels with $J = 1/2, 3/2$ and 5/2 from which the 300 lowest were considered in the second-step lifetime calculations. The same configurations for each $n = 5, 6, 7$ also give rise to 310 levels with $J = 7/2, 9/2$ and 11/2, from which the lowest 300 were also considered for each n. A similar size of the expansion has been used also for the final states. Here, the inclusion of all CSF with $J = 0$, 1 and 2 from the four configurations $4s\,4p^5$, $4s^2\,4p^4$, $4s^2\,4p^2\,4d^2$ and $4s^2\,4p^2\,5p^2$ yields a total of 128 CSF.

The Auger amplitudes of all considered transitions were calculated by means of the RATIP package [27], in which the continuum orbitals are obtained within a spherical and level-dependent potential of the (corresponding) final-ionic bound state, a scheme that includes the exchange interaction of the emitted electron with the bound-state density [28]. Once the amplitudes are known, the Auger rates for all transitions can be calculated in the usual way.

Since we are mainly interested in the cascades of Auger transitions, we concentrate on the part of the Auger spectrum that corresponds to the $M_{4,5}N_1N_1$ and $M_{4,5}N_1N_{2,3}$ diagram transitions and the corresponding resonant Auger transitions, which can be followed by the second-step Auger decay (see figure 1). The calculated spectrum of the normal Auger decay (first step) agrees very well with the experimental data and calculations presented in [10, 12]. Due to energy considerations, the second-step Auger transition to the final states of Kr^{3+} is possible only for a few high-lying excited states of Kr^{2+} that are weakly populated. Besides, the calculated lifetime of these transitions is small, of the order of 0.1 fs or even less. Such a fast decay is typical of super-Coster–Kronig transitions when all participating electrons belong to the same shell (for example, $4s\,4p^5 \rightarrow 4s^2\,4p^3$). A fast transition means a broad line (about 6–7 eV). Therefore, these weak and broad lines can hardly be discerned in the experiment and contribute to the background.

Different insights emerge from the calculations for the resonant Auger transitions. The calculated spectra of the first step transitions for $n = 5$ are close to those calculated in [13, 15]. The spectra agree satisfactorily with the experimental data [14], at least for the diagram transitions to the 4s $4p^5$ 5p configuration (the deviation of calculated energy is not larger than 0.4 eV). For strong correlation satellites, transitions to the levels with dominant configuration $4s^2\,4p^3$ 4d 5p, the agreement is worse (the calculated transition energies are lower than the experimental ones by 3–4 eV). Even larger deviations occur for the level energies of the $4s^0\,4p^6$ 5p configuration with two 4s holes in the final states. Here, the MCDF calculations underestimate the transition energy by as much as 9 eV. These deviations arise for two reasons: (i) the strong coupling of the 4s hole states to the electron continuum due to allowed (super-) Coster–Kronig transitions and (ii) the incomplete mixing of these levels in the given CSF basis. The shift of the energy levels caused by the continuum, also known as *interchannel interaction* in the literature, can be several eV for hole states and usually comes together with a large width and a short lifetime of the levels [29]. A small theoretical transition energy of the first-step Auger transitions to these levels is mainly caused by the calculated final states that are too high in energy and which then become the initial states for the second-step Auger transitions. Thus one can expect that the calculated energies of the second step transitions have a rather large uncertainty of several eV.

In tables 1–3, we present the calculated results for the selected second-step transitions in Kr (3d) cascades initiated by 5p, 6p and 7p excitations, respectively. Shown in the tables are the energy of the initial state of the Kr^+ ion relative to the ground state $4s^2\,4p^4\,{}^3P_2$ of the Kr^{2+}, the initial and final state dominant configurations, Auger lifetime and the energies of the dominant decay channels. We selected the transitions from those initial states that are populated most strongly by the first-step Auger transitions. Since the second step in the cascade is a participator transition in which the outer Rydberg electron is involved, the Auger lifetime is much larger than for normal Auger transitions and increases with increasing n. This tendency is preserved also for excitation of higher Rydberg resonances (larger n). However, their contribution should diminish due to a rapid decrease in the photoexcitation cross section.

4. Experimental results and discussion

Using the schematic energy diagram (figure 1), it is possible to identify which of the observed Auger lines have to belong to the first step of the Auger decay (normal and resonant) and which may possibly be emitted in the second step of the Auger cascade. In the case where the XUV pulse with an energy of about 94 eV ionizes from the 3d subshell, the electrons with a kinetic energy higher than ∼20 eV must be first-step normal Auger electrons, because the threshold for triple ionization of krypton lies at ∼74.4 eV [18]. For resonant transitions, Auger electrons with a kinetic energy higher than ∼35 eV can be clearly assigned to be first-step Auger electrons. Thus the second-step Auger electrons, which are of our primary interest, can be expected at lower energies. Figure 4 shows the low-energy part of the measured spectrum when the IR probe arrives before the XUV pump pulse. As in figure 3, the vertical bars indicate the position of the previously observed first-step (resonant—dashed magenta with stars—and normal—solid red with dots) and second-step resonant Auger lines (fine dashed green with triangles).

In our pump–probe experiment, sidebands to the Auger lines appear when the Auger emission overlaps in time with the IR probe pulse, which can be clearly seen in the inset of figure 4. In order to determine the relaxation time of the different steps of the cascaded Auger

Table 1. Calculated Auger lifetimes and electron kinetic energies for the dominant decay channels of the second step transitions in Auger cascades initiated by an $3d^{-1}5p$ excitation in Kr. The excitation energies of the Kr^+ intermediate states are given relative to the ground state $4p^4\ ^3P_2$ of Kr^{2+}. Only the dominant configuration in the multiconfiguration wave function of the initial and final states is given.

Number	Initial config.	Final config.	Initial energy (eV)	Lifetime (fs)	Transition energy (eV)
1	$4s4p^5\ 5p$	$4s^2\ 4p^4$	6.82	4.54	6.82
2	$4s4p^5\ 5p$	$4s^2\ 4p^4$	7.06	3.56	6.51; 6.40
3	$4s4p^5\ 5p$	$4s^2\ 4p^4$	7.34	3.88	7.34; 6.80; 6.68
4	$4s4p^5\ 5p$	$4s^2\ 4p^4$	7.38	4.22	7.38; 6.83; 6.72
5	$4s4p^5\ 5p$	$4s^2\ 4p^4$	7.66	3.24	7.11
6[a]	$4s4p^5\ 5p$	$4s^2\ 4p^4$	10.20	4.14	10.20; 9.66; 8.04
7[a]	$4s4p^5\ 5p$	$4s^2\ 4p^4$	10.27	2.86	10.27; 9.72; 8.10
8	$4s4p^5\ 5p$	$4s^2\ 4p^4$	10.49	4.87	10.49; 9.98; 9.83; 8.33
9	$4s^2\ 4p^3\ 4d\ 5p$	$4s^2\ 4p^4$	17.91	0.25	
10	$4s^2\ 4p^3\ 4d\ 5p$	$4s^2\ 4p^4$	18.04	0.58	
11	$4s^2\ 4p^3\ 4d\ 5p$	$4s^2\ 4p^4$	18.29	10.85	18.29; 17.63; 16.12; 7.09
12[a]	$4s^2\ 4p^3\ 4d\ 5p$	$4s^2\ 4p^4$	19.41	4.89	19.41; 18.86; 18.75; 17.24
13[a]	$4s^2\ 4p^3\ 4d\ 5p$	$4s^2\ 4p^4$	19.46	3.78	19.46; 18.91; 18.80; 17.29
14	$4s^2\ 4p^3\ 4d\ 5p$	$4s^2\ 4p^4$	19.60	3.57	19.60; 19.06; 17.44
15	$4s^2\ 4p^3\ 4d\ 5p$	$4s^2\ 4p^4$	19.63	0.40	
16	$4s^2\ 4p^3\ 4d\ 5p$	$4s^2\ 4p^4$	19.70	0.81	
17	$4s^2\ 4p^3\ 4d\ 5p$	$4s^2\ 4p^4$	19.80	0.47	
18[a]	$4s^2\ 4p^3\ 4d\ 5p$	$4s^2\ 4p^4$	21.68	3.22	21.68; 21.14; 21.02; 19.52; 17.09
19[a]	$4s^2\ 4p^3\ 4d\ 5p$	$4s^2\ 4p^4$	21.72	7.74	21.72; 21.17; 19.55; 17.13
20	$4s^2\ 4p^3\ 4d\ 5p$	$4s^2\ 4p^4$	21.77	16.66	21.77; 19.60
21	$4s^2\ 4p^3\ 4d\ 5p$	$4s^2\ 4p^4$	21.86	2.29	21.86; 19.69
22	$4s^04p^6\ 5p$	$4s\ 4p^5$	32.40	1.53	14.82; 7.64
23[a]	$4s^04p^6\ 5p$	$4s\ 4p^5$	32.48	1.54	7.71

[a]Those levels that are populated with the highest probability by the first-step Auger transition.

decay, we measure the intensity of the Auger lines and generated sidebands as a function of the pump-probe delay. In order to improve statistics we group together lines that can be expected to show the same temporal behavior. All Auger lines and corresponding sidebands with a kinetic energy above ∼35 eV can be grouped together since these are strictly emitted in the first step of the Auger decay (at these high energies, the only step). We note that within the experimental accuracy of our measurements, the normal Auger decay of the 3d vacancy and resonant Auger decay of $3d^{-1}np$ excited states have the same lifetime (compare the results of measurements in [2] and [30]). Therefore, we included them in the same group. At lower energies Auger lines are grouped together in the intervals 23–27 eV (see figure 4) and 28–34 eV. The most prominent lines at even lower kinetic energies are treated individually.

The intensity of the emitted Auger lines and corresponding sidebands was fitted for each spectrum taken at different pump–probe delays. The relaxation time of the first-step Auger

Table 2. Calculated Auger lifetimes and electron kinetic energies for the dominant decay channels of the second step transitions in Auger cascades initiated by an $3d^{-1}6p$ excitation in Kr. The excitation energies of the Kr^+ intermediate states are given relative to the ground state $4p^4\,{}^3P_2$ of Kr^{2+}. Only the dominant configuration in the multiconfiguration wave function of the initial and final states is given.

Number	Initial config.	Final config.	Initial energy (eV)	Lifetime (fs)	Transition energy (eV)
1	$4s4p^5\ 6p$	$4s^2\ 4p^4$	10.20	15.89	10.20
2	$4s4p^5\ 6p$	$4s^2\ 4p^4$	10.28	13.66	10.28; 9.73; 9.62; 8.08
3	$4s4p^5\ 6p$	$4s^2\ 4p^4$	10.59	17.41	10.59; 10.04; 8.39
4	$4s4p^5\ 6p$	$4s^2\ 4p^4$	10.62	14.33	10.62; 10.08; 9.96; 8.42
5	$4s4p^5\ 6p$	$4s^2\ 4p^4$	10.89	14.10	10.35; 10.23; 8.70; 6.20
6[a]	$4s4p^5\ 6p$	$4s^2\ 4p^4$	13.65	14.70	13.65; 13.11; 12.99; 11.46
7[a]	$4s4p^5\ 6p$	$4s^2\ 4p^4$	13.68	11.20	13.68; 13.14; 11.48; 8.98
8	$4s4p^5\ 6p$	$4s^2\ 4p^4$	13.76	15.20	13.21; 13.10; 11.56
9	$4s^2\ 4p^3\ 4d\ 6p$	$4s^2\ 4p^4$	21.32	0.18	
10	$4s^2\ 4p^3\ 4d\ 6p$	$4s^2\ 4p^4$	21.34	0.37	
11	$4s^2\ 4p^3\ 4d\ 6p$	$4s^2\ 4p^4$	21.40	0.23	
12	$4s^2\ 4p^3\ 4d\ 6p$	$4s^2\ 4p^4$	21.68	0.13	
13	$4s^2\ 4p^3\ 4d\ 6p$	$4s^2\ 4p^4$	22.79	26.0	22.79; 22.25; 22.13; 20.60
14[a]	$4s^2\ 4p^3\ 4d\ 6p$	$4s^2\ 4p^4$	22.80	17.60	22.80; 22.26
15	$4s^2\ 4p^3\ 4d\ 6p$	$4s^2\ 4p^4$	22.85	27.55	20.65
16	$4s^2\ 4p^3\ 4d\ 6p$	$4s^2\ 4p^4$	22.85	13.11	22.85; 20.65
17	$4s^2\ 4p^3\ 4d\ 6p$	$4s^2\ 4p^4$	22.86	6.27	20.66
18	$4s^2\ 4p^3\ 4d\ 6p$	$4s^2\ 4p^4$	22.91	7.02	22.91; 22.37; 22.25; 20.72; 18.22
19	$4s^2\ 4p^3\ 4d\ 6p$	$4s^2\ 4p^4$	22.94	4.05	22.94; 22.40; 22.28; 20.75; 18.25
20	$4s^2\ 4p^3\ 4d\ 6p$	$4s^2\ 4p^4$	25.06	0.12	
21[a]	$4s^2\ 4p^3\ 4d\ 6p$	$4s^2\ 4p^4$	25.07	0.13	
22	$4s^2\ 4p^3\ 4d\ 6p$	$4s^2\ 4p^4$	25.08	0.14	
23	$4s^2\ 4p^3\ 4d\ 6p$	$4s^2\ 4p^4$	25.11	0.14	19.8; 19.3
24	$4s^0\ 4p^6\ 6p$	$4s\ 4p^5$	35.73	4.02	18.32; 11.13
25[a]	$4s^0\ 4p^6\ 6p$	$4s\ 4p^5$	35.76	4.10	11.16

[a]Those levels that are populated with the highest probability by the first-step Auger transition.

decay is obtained by fitting a convolution of the system response (i.e. the IR probe envelope convoluted with the attosecond pulse) with an exponential decay. The cascaded Auger relaxation times are obtained by fitting a convolution of the first-step Auger decay and system response (to describe the population of the intermediate state) with an exponential decay. Below we discuss the results of such an analysis for several groups of lines.

In figure 5 we show the observed intensity of the Auger lines with a kinetic energy between 35 and 48 eV and the corresponding sidebands, together with a fit to the observed kinetics. The intensities of all Auger lines with a kinetic energy above ∼35 eV (solid red circles) and the corresponding sidebands (open red circles) show the same behavior, and the fits (dashed and solid red lines) of an exponential decay convoluted with the IR probe envelope yield the same

Table 3. Calculated Auger lifetimes and electron kinetic energies for the dominant decay channels of the second step transitions in Auger cascades initiated by an $3d^{-1}7p$ excitation in Kr. The excitation energies of the Kr^+ intermediate states are given relative to the ground state $4p^4\,{}^3P_2$ of Kr^{2+}. Only the dominant configuration in the multiconfiguration wave function of the initial and final states is given.

Number	Initial config.	Final config.	Initial energy (eV)	Lifetime (fs)	Transition energy (eV)
1	$4s4p^5\ 7p$	$4s^2\ 4p^4$	11.65	27.99	11.65
2	$4s4p^5\ 7p$	$4s^2\ 4p^4$	11.69	24.42	11.69; 11.14; 11.03; 9.49; 6.98
3	$4s4p^5\ 7p$	$4s^2\ 4p^4$	12.06	24.79	12.06; 11.52; 11.40; 9.86; 7.36
4	$4s4p^5\ 7p$	$4s^2\ 4p^4$	12.07	24.38	12.07; 11.53; 11.41; 9.88; 7.37
5	$4s4p^5\ 7p$	$4s^2\ 4p^4$	12.32	26.01	12.32; 11.78; 11.66; 10.12; 7.62
6[a]	$4s4p^5\ 7p$	$4s^2\ 4p^4$	15.13	23.46	15.13; 14.59; 14.47; 12.93
7[a]	$4s4p^5\ 7p$	$4s^2\ 4p^4$	15.14	17.94	15.14; 14.60; 12.95; 10.44
8	$4s4p^5\ 7p$	$4s^2\ 4p^4$	15.17	22.55	15.17; 14.63; 12.97
9	$4s4p^5\ 7p$	$4s^2\ 4p^4$	15.18	22.69	15.18; 14.64; 14.52; 12.98
10	$4s^2\ 4p^3\ 4d\ 7p$	$4s^2\ 4p^4$	22.79	0.49	
11	$4s^2\ 4p^3\ 4d\ 7p$	$4s^2\ 4p^4$	22.80	0.83	
12	$4s^2\ 4p^3\ 4d\ 7p$	$4s^2\ 4p^4$	23.14	0.37	
13	$4s^2\ 4p^3\ 4d\ 7p$	$4s^2\ 4p^4$	23.40	0.41	
14	$4s^2\ 4p^3\ 4d\ 7p$	$4s^2\ 4p^4$	24.27	60.62	24.27; 23.72; 23.61; 22.07; 6.42
15[a]	$4s^2\ 4p^3\ 4d\ 7p$	$4s^2\ 4p^4$	24.27	52.68	24.27; 23.73; 6.42
16	$4s^2\ 4p^3\ 4d\ 7p$	$4s^2\ 4p^4$	24.29	7.31	22.09
17	$4s^2\ 4p^3\ 4d\ 7p$	$4s^2\ 4p^4$	24.34	12.61	24.34; 23.80; 23.68; 22.14; 19.63
18[a]	$4s^2\ 4p^3\ 4d\ 7p$	$4s^2\ 4p^4$	26.53	0.55	
19	$4s^2\ 4p^3\ 4d\ 7p$	$4s^2\ 4p^4$	26.53	0.58	
20	$4s^2\ 4p^3\ 4d\ 7p$	$4s^2\ 4p^4$	26.54	0.54	
21[a]	$4s^0\ 4p^6\ 7p$	$4s\ 4p^5$	37.19	8.55	12.61

[a]Those levels that are populated with the highest probability by the first-step Auger transition.

time constant (8 ± 1 fs) for both the sideband and the Auger line, in agreement with the literature value for the first step of the Auger decay [2, 4]. This confirms that the signal from the Auger electrons for our experimental conditions can be used to determine the relaxation time.

For the group of Auger lines with the energy 28–34 eV, our experimental data show the same behavior as for the higher-energy Auger electrons; thus this group can also be attributed to the first-step Auger transitions. However, the group of lines around 25 eV and lower-energy lines show different dependences on the time delay.

Figure 6 shows the observed intensity of the Auger peak(s) at ~12 eV, which corresponds presumably to the second-step transition, together with a fit to the experimental data. Since no sideband corresponding to the low-energy Auger peak (at ~12 eV) is resolved, the decay time of the second step of the Auger decay can only be determined from the decrease in signal in the Auger peak. It is important to note that, from previous work [4], it is known that the decrease in signal in the Auger peak does not necessarily correspond exactly to the increase in signal in the sideband, when the probe intensity is too high, due to the formation of sidebands of multiple

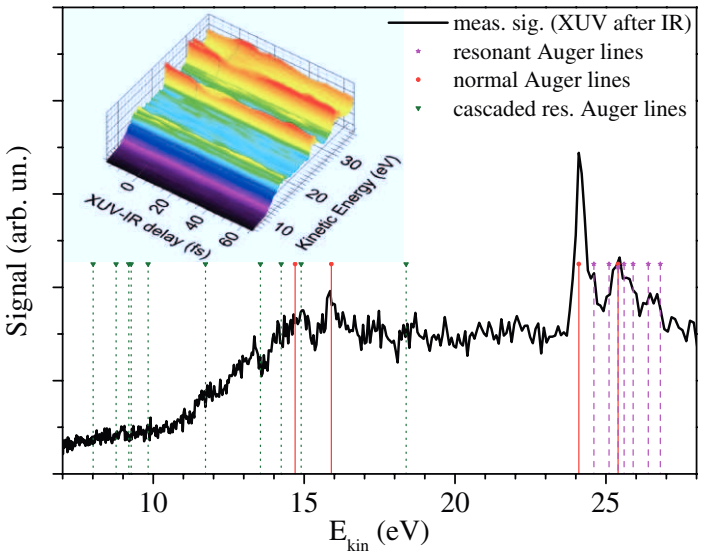

Figure 4. Low-energy part of the spectrum measured with the IR probe timed well before the XUV pump pulse. The positions of the most prominent known Auger lines are indicated by the vertical solid red lines and dots (normal Auger) [10, 12] and dashed magenta lines and stars (resonant Auger) [14]. The vertical short dashed green lines and triangles indicate the positions of the cascaded resonant Auger emission lines observed in [15, 17]. Inset: the low-energy part of the spectrum plotted versus pump–probe delay. With the help of this plot, one can more easily identify low-energy features in the spectrum.

orders. In our experiment, we set the IR probe intensity such that only one sideband of the higher energy Auger peaks was generated. The decay time, derived from the signal in the 12 eV Auger peak (open green circles in figure 6), is fitted to be 74 ± 20 fs (solid green line in figure 6). Since this lifetime is much larger than the lifetime of normal or resonant (first-step) Auger decay, one can affirm that the line corresponds to the second-step Auger transition, most probably from the resonance $3d^{-1}np$ with $n = 7$ or higher, according to our theoretical analysis.

Our experimental data for the group of lines with 23–27 eV consistently show a delayed appearance of the sidebands to the Auger electrons with a kinetic energy around 25 eV (see figure 7). In this energy interval, two normal Auger lines (24.15 and 25.41 eV) have been observed [12], which were attributed to the $M_{4,5}N_1N_1$ transitions. Also in resonant Auger spectra several transitions have been observed in this energy interval which were attributed to the first-step resonant Auger transitions [14]. The delayed emission of the electrons around 25 eV indicates that at least some of these electrons are emitted in a second step in the Auger decay following excitation to a Rydberg state from the 3d subshell and a first step resonant Auger decay. Analyzing the results of our calculations shown in tables 1–3, one can admit that the delayed electrons are emitted in a second step of the cascade following a correlation satellite $4s^2\,4p^3\,4d6p \rightarrow 4s^2 4p^4$ emission in a resonant Auger transition. In fact, the same transition is presumably probed in [7], although there no clear assignment of the states involved could be made. We note that in the considered case it is not trivial to extract the relaxation time of the second resonant Auger decay. As shown in figure 7, the data (black open circles) are fitted to the sum of two decays (black curve): the result of the fit of the Auger lines in the kinetic

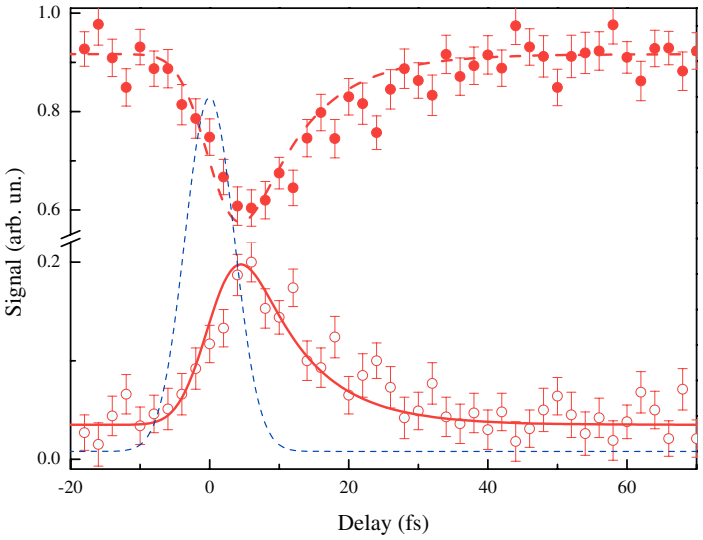

Figure 5. Extracted intensity of the ensemble of Auger lines (filled red circles) and corresponding sidebands (open red circles) in a kinetic energy range from 35 eV to 48 eV and fits to the experimental data (dashed and solid red lines, respectively). The extracted relaxation time τ_1 is 8 ± 1 fs. The result from this fit is used as a fixed parameter in the fits performed to obtain the relaxation time of the second step in the (resonant) Auger decay. The dashed blue line shows the IR amplitude envelope.

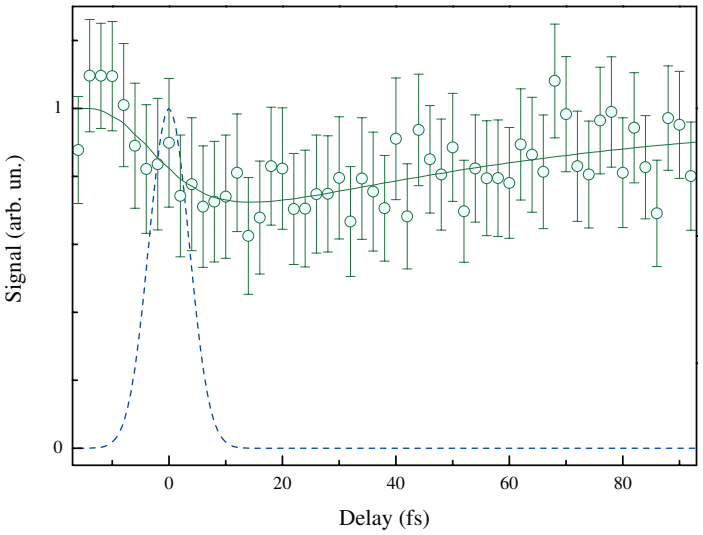

Figure 6. Extracted intensity of the second-step Auger line observed at a kinetic energy of about 12 eV. The solid green line shows the best fit to the data. The extracted relaxation time τ_2 is 74 ± 20 fs. The dashed blue line shows the IR amplitude envelope.

energy range from 35 to 48 eV with its amplitude as a free fit parameter (dotted red curve) and a second-step resonant Auger decay (dash-dotted green curve), using an 8 fs relaxation time for the first step of the Auger decay. In the fit, the parameters obtained in the fit of the first step of

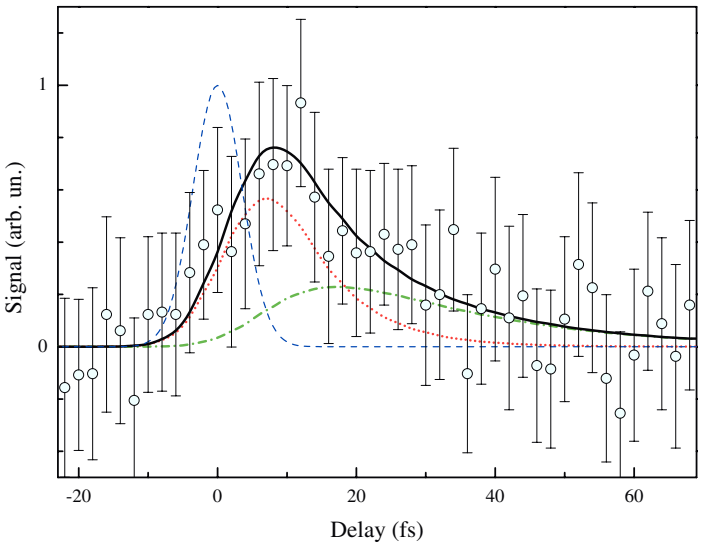

Figure 7. Extracted intensity of the ensemble of sidebands belonging to the Auger lines observed with a kinetic energy between 23 and 27 eV. The red and green lines show the two components: dotted red—first-step (from both resonant and normal) Auger decay, determined by the fit shown in figure 5—and dash-dotted green—second-step (only from resonant) Auger decay, adding up to the fitted total sideband intensity (black line). The extracted decay time τ_2 for the delayed transition is 26 ± 4 fs. The dashed blue line shows the IR amplitude envelope.

the Auger decay are fixed (i.e. the relaxation time τ_1 and the system response function), while the relaxation time of the cascaded Auger decay τ_2 and the strengths of both the first and the second decay are free parameters. This yields a relaxation time of 26 ± 4 fs for the second step of the resonant Auger decay (dash-dotted green curve), which is in good agreement with [7].

5. Conclusions

Using electron time-of-flight spectrometry in an XUV pump–IR probe experiment, we have energy- and time-resolved for the first time the cascaded Auger decay following XUV excitation and ionization of the Kr 3d subshell. The observed large decay time of 74 ± 20 fs of the Auger electrons with a kinetic energy around 12 eV can be attributed to the second-step transitions in a resonant Auger cascade with possible assignment $4s4p^5np \rightarrow 4s^2 4p^4$ or $4s^2\,4p^3\,4dnp \rightarrow 4p^4$ with $n = 7$ or higher, according to our theoretical calculations. Our data suggest that Auger electrons that are emitted with a kinetic energy of $\sim$25 eV have a component with a relaxation time of 26 ± 4 fs. The corresponding electrons are presumably emitted in a second step of the cascaded resonant Auger decay. Our investigation, supported by the findings in [7], suggests an assignment of $4s^2\,4p^3\,4dnp \rightarrow 4p^4$ with $n = 6, 7$ for this component. The present experiment shows that attosecond electron spectroscopy has evolved from the proof-of-principle experiment in [4] to a level where complex processes are resolved in time that cannot be accessed using any other technique currently available.

Acknowledgments

This work was supported by the Austrian Science Fund (grant no. U33-N16) and the German Ministry for Education and Research (grant no. 05KS7GU4). NMK acknowledges the hospitality of the Institut für Photonik, Technische Universität Wien, extended to him during his visit.

Appendix

A.1. Fit procedure

We fit the experimentally measured spectra for each pump-probe delay (t) by using the following expression:

$$\begin{aligned} I(t) = c/W^{\mathrm{ph}}(t) \sum_i a_i^{\mathrm{ph}} \exp\left(-(x - p_i^{\mathrm{ph}})^2/W^{\mathrm{ph}}(t)^2\right) \\ + \sum_j \left\{ A_j^{\mathrm{Au}}(t) \sum_k a_{j,k}^{\mathrm{Au}} \exp\left(-(x - p_{j,k}^{\mathrm{Au}})^2/{w_{j,k}^{\mathrm{Au}}}^2\right) \right. \\ + A_j^{\mathrm{sAu}}(t) \left[\sum_k a_{j,k}^{\mathrm{Au}} \exp\left(-(x - p_{j,k}^{\mathrm{Au}} - 1.6)^2/{w_{j,k}^{\mathrm{Au}}}^2\right) \right. \\ \left. \left. + \sum_k a_{j,k}^{\mathrm{Au}} \exp\left(-(x - p_{j,k}^{\mathrm{Au}} + 1.6)^2/{w_{j,k}^{\mathrm{Au}}}^2\right) \right] \right\} \\ + \text{background}, \end{aligned} \tag{A.1}$$

with $W^{\mathrm{ph}}(t)$ being the width of the valence electron photoemission, c is a normalization constant that is obtained from the relation between the height and width of the photoemission peaks and the conservation of the number of electrons observed in the photoemission, $A_j^{\mathrm{Au}}(t)$ is the relative amplitude of the jth group of Auger lines $A_j^{\mathrm{sAu}}(t)$ is the relative amplitude of the corresponding sidebands. The parameters denoted by lower case letters are:

a_i^{ph}, p_i^{ph}	relative strengths and positions of the direct photoemission lines and possible shake-up lines.
$a_{j,k}^{\mathrm{Au}}$, $p_{j,k}^{\mathrm{Au}}$, $w_{j,k}^{\mathrm{Au}}$	relative strengths, position and widths of the Auger lines in the jth group. In our spectra the widths of the observed Auger lines are determined by the spectrometer resolution rather than by their natural line width.

The last two sums in expression (A.1) describe the contribution of the sidebands, with 1.6 eV being the energy of the IR photon.

The background is mostly due to a large number of additional shake-up photo-lines [31]. The streaking of these lines is barely visible, because of the high number of overlapping spectral features. We found that keeping the background constant over all delays did not influence the results, although a small variation of the background would be expected as a result of streaking around zero delay.

We process the experimental data according to the following steps.

(i) First we fit the spectrum for the case when the XUV pulse is as long as possible after the IR; thus the IR pulse does not affect the spectrum (see, e.g., figure 3, where the delay $t = t_m < -10$ fs). For this fit we use equation (A.1) with $c/W^{\mathrm{ph}}(t_m) = 1$, the relative amplitude of the groups of Auger lines $A_j^{\mathrm{Au}}(t_m) = 1$, the relative amplitude of the corresponding sidebands $A_j^{\mathrm{sAu}}(t_m) = 0$, to get the initial value of the direct photoelectron emission width W^{ph} and to fix the values of the lower-case parameters. We perform this fit by hand, estimating the relative strengths of neighboring lines using [9, 12–14]. Of course the positions of the lines should more or less coincide with the tabulated line positions in the literature [9, 10, 12–14]. However, it is not possible to reconcile the line positions with all referenced literature sources at once. Thus, the time-of-flight spectrometer is calibrated using the tabulated line positions from [12], and the line positions from the other literature sources are shifted (per source, maximum applied shift 0.4 eV) to match the observed line positions rather than that the line positions are used as a free parameter. Since the spectrum of the XUV pulses covers both transitions from the 3d subshell to Rydberg states and to the continuum, the Auger spectrum contains lines that can be attributed to the normal Auger decay [9, 10, 12] and the resonant Auger decay [13, 14]. Thus all lines above a kinetic energy of ∼15 eV we observe in the spectrum can be assigned, and the observed line positions match within our experimental precision.

(ii) We fit the spectrum for each delay using equation (A.1) with the parameters denoted by upper-case letters free, and the parameters denoted by lower-case letters fixed according to the previous step. This yields $W^{\mathrm{ph}}(t)$, and all $A_j^{\mathrm{Au}}(t)$ and $A_j^{\mathrm{sAu}}(t)$. In principle, an additional fidelity test of the fit can be made, using the (reasonable) assumption that the number of electrons in each group should be conserved. So one may check that $A_j^{\mathrm{Au}}(t) + 2A_j^{\mathrm{sAu}}(t) = 1$. Since the sidebands are obviously found at slightly different kinetic energies than the 'mother'-lines, this step intrinsically assumes a reasonably flat spectral throughput as a function of kinetic energy. This holds best for higher kinetic energies, and we found it practically applicable for all energies above ∼20 eV.

(iii) Having $W^{\mathrm{ph}}(t)$, we can use this to get the system-response or IR envelope, using a simple Gaussian fit:

$$A_{\mathrm{ph}}(t) = a_{\mathrm{ph}} \exp\left(-(t/\Delta)^2\right). \tag{A.2}$$

The only parameter of interest to us from this fit is the duration, Δ. If a clear IR pre- or post-pulse can be seen in $W^{\mathrm{ph}}(t)$, the data cannot be used, because the pre- or post-pulses will induce more sideband formation, and the data analysis depends strongly on a correct description of the IR probe pulse. Of course, the occurrence of pre- or post pulses can actually easily be seen in the raw data, so data with clear IR satellites are immediately discarded.

(iv) To get the first Auger lifetime, we fit $1 - A_1^{\mathrm{Au}}(t)$ and $A_1^{\mathrm{sAu}}(t)$ to the equation [4]

$$A_1(t) = a_1 \int \exp\left(-((t - T - t')/\Delta)^{2\alpha}\right) D(t, \tau_1)\, \mathrm{d}t', \tag{A.3}$$

where $D(t, \tau) = \left[\exp(-t/\tau)_{t>0}, 0_{t<0}\right]$ with Δ as found in the previous step, and using the same procedure as in [4] to find the optimal value for $\alpha = 0.4$. Correct calibration of the zero delay requires that $T = 0$. A nonzero (positive) value of T would implicate that the decay starts not immediately after the excitation.

(v) To determine whether the second Auger group is a decay from the same excited state or from a different excited state (or a cascade), we perform a fit of $1 - A_2^{\mathrm{Au}}(t)$ and $A_2^{\mathrm{sAu}}(t)$ using equation (A.3). If this yields a different τ_1, but looks fine with the same T, the most reasonable explanation would be that the decay is from a different excited state. (There could be, for example, a difference between normal Auger and resonant Auger transitions. This difference can be neglected in the case of krypton.) If the fit requires a significantly different T, no matter τ_1, this means that the electrons are emitted later (or earlier, but that will not be the case here). In that case, to get the second Auger lifetime, we fit $1 - A_2^{\mathrm{Au}}(t)$ and $A_2^{\mathrm{sAu}}(t)$ to

$$A_2(t) = a_2 \int \left[\exp\left(-((t - T - t'')/\Delta)^{2\alpha}\right) \int D(t - t', \tau_1) D(t, \tau_2)\, \mathrm{d}t' \right] \mathrm{d}t'' \tag{A.4}$$

with T, Δ, α and τ_1 fixed (obtained from the fit of $1 - A_1^{\mathrm{Au}}(t)$ and $A_1^{\mathrm{sAu}}(t)$).

The second Auger group can consist of overlapping lines of different origin. This means, for example, that part of the signal originates from the first Auger decay, and part from a cascade in the resonant Auger decay. The second Auger lifetime can be obtained by fitting the sum of equations (A.3) and (A.4). In that case the T, Δ, α and τ_1 are fixed, and through the parameters a_1 and a_2 the relative contributions of the two different decays to the total signal can be obtained.

A.2. Error bars

The error bars for our experimental data are computed straightforwardly: the error for each datapoint in our time-of-flight spectra is determined by the Poisson-statistics, since we count individual electrons hitting the detector. When we fit our spectra, we use the Levenberg–Marquardt fit routine in LabVIEW 8.2, and provide the measured data points together with the corresponding weighting factors (i.e. inverse error bars), to obtain three sets of output data: (i) the fitted spectrum; (ii) the fitted values of the coefficients (here the upper-case parameters in equations (A.1); and (iii)) the covariance matrix. The error bars of the fitted coefficients are derived from the covariance matrix.

The Auger lifetimes are fitted using the Levenberg–Marquardt fit algorithm in Mathcad 14, using the model functions in equations (A.3) and (A.4), or the sum of these two functions, as described above, providing the data points and error bars calculated in the previous step. The error bars for each of the fit parameters are then provided as well by this algorithm.

References

[1] Aksela H, Aksela S and Kabachnik N M 1996 *VUV and Soft X-Ray Photoionization* ed U Becker and D A Shirley (New York: Plenum) chapter 11

[2] Jurvansuu M, Kivimäki A and Aksela S 2001 Inherent lifetime widths of Ar $2p^{-1}$, Kr $3d^{-1}$, Xe $3d^{-1}$, and Xe $4d^{-1}$ states *Phys. Rev.* A **64** 012502

[3] Kabachnik N M, Fritzsche S, Grum-Grzhimailo A M, Meyer M and Ueda K 2007 Coherence and correlations in photoinduced Auger and fluorescence cascades in atoms *Phys. Rep.* **451** 155

[4] Drescher M, Hentschel M, Kienberger R, Uiberacker M, Yakovlev V, Scrinzi A, Westerwalbesloh T, Kleineberg U, Heinzmann U and Krausz F 2002 Time-resolved atomic inner-shell spectroscopy *Nature* **419** 803

[5] Drescher M, Hentschel M, Kienberger R, Uiberacker M, Westerwalbesloh T, Kleineberg U, Heinzmann U and Krausz F 2004 Time-resolved electron spectroscopy of atomic inner-shell dynamics *J. Electron Spectrosc. Relat. Phenom.* **137** 259

[6] Uiberacker M *et al* 2007 Attosecond real-time observation of electron tunnelling in atoms *Nature* **446** 627

[7] Uphues T, Schultze M, Kling M, Uiberacker M, Hendel S, Heinzmann U, Kabachnik N M and Drescher M 2008 Ion-charge-state chronoscopy of cascaded atomic Auger decay *New J. Phys.* **10** 025009

[8] Mehlhorn W, Schmitz W and Stalherm D 1972 Korrelationseffekte in den Auger-Spektren von Edelgasen *Z. Phys.* **252** 399

[9] Werme L, Bergmark T and Siegbahn K 1972 The high resolution $L_{2,3}MM$ and $M_{4,5}NN$ Auger spectra from krypton and $M_{4,5}MM$ and $N_{4,5}OO$ Auger spectra from xenon *Phys. Scr.* **6** 141

[10] Aksela H, Aksela S and Pulkkinen H 1984 Correlation effects in $4s^0\,4p^6$ and $4s^1\,4p^5$ configurations of krypton studied by the M-NN Auger decay *Phys. Rev.* A **30** 2456

[11] Heimann P *et al* 1987 Shake-off on inner-shell resonances of Ar, Kr and Xe *J. Phys. B: At. Mol. Opt. Phys.* **20** 5005

[12] Jauhiainen J, Aksela H, Aksela S, Kivimäki A, Sairanen O P, Nõmmiste E and Vegh J 1995 Correlation satellites in the Xe $N_{4,5}$–OO and Kr $M_{4,5}$–NN Auger spectra *J. Phys. B: At. Mol. Opt. Phys.* **28** 3831

[13] Aksela H, Jauhiainen J, Kukk E, Nõmmiste E, Aksela S and Tulkki J 1996 Electron correlation in the decay of resonantly excited $3d^{-1}_{3/2,5/2}5p$ states of krypton *Phys. Rev.* A **53** 290

[14] Mursu J, Jauhiainen J, Aksela H and Aksela S 1998 High resolution study of correlation satellites in the $M_{4,5}$–$N_1N_{2,3}$ resonant Auger spectra of Kr *J. Phys. B: At. Mol. Opt. Phys.* **31** 1973

[15] Kitajima M *et al* 2001 Experimental and theoretical study of the Auger cascade following $3d \rightarrow 5p$ photoexcitation in Kr *J. Phys. B: At. Mol. Opt. Phys.* **34** 3829

[16] Brünken S, Gerth C, Kanngießer B, Luhmann T, Richter M and Zimmermann P 2002 Decay of the Ar $2s^{-1}$ and $2p^{-1}$ and Kr $3p^{-1}$ and $3d^{-1}$ hole states studied by photoelectron-ion coincidence spectroscopy *Phys. Rev.* A **65** 042708

[17] von Raven E, Meyer M, Paler M and Sonntag B 1990 Electron–electron coincidence studies of the decay of photoexcited rare gas core resonances *J. Electron Spectrosc. Relat. Phenom.* **52** 677

[18] Viefhaus J, Braune M, Korica S, Reinköster A, Rolles D and Becker U 2005 Auger cascades versus direct double Auger: relaxation processes following photoionization of the Kr 3d and Xe 4d, 3d inner shells *J. Phys. B: At. Mol. Opt. Phys.* **38** 3885

[19] Kienberger R *et al* 2004 Atomic transient recorder *Nature* **427** 817

[20] Verhoef A J, Mitrofanov A V, Nguyen X T, Krikunova M, Fritzsche S, Kabachnik N M, Drescher M and Baltuška A 2011 Time-and-energy resolved measurement of the cascaded auger decay in Krypton *Laser Phys.* **21** 1270

[21] Tulkki J, Aksela H and Kabachnik N M 1994 Influence of the initial- and final-state configuration interaction on the anisotropy of the resonant Auger decay of Kr $3d^{-1}5p$ and Xe $4d^{-1}6p$ states *Phys. Rev.* A **50** 2366

[22] Grant I 1988 Relativistic effects in atoms and molecules *Methods in Computational Chemistry* ed S Wilson vol 2 (New York: Plenum) p 1

[23] Parpia F, Froese Fischer C and Grant I 1996 GRASP92: a package for large-scale relativistic atomic structure calculations *Comput. Phys. Commun.* **94** 249

[24] Fritzsche S, Froese Fischer C and Gaigalas G 2002 RELCI: a program for relativistic configuration interaction calculations *Comput. Phys. Commun.* **148** 103

[25] Fritzsche S, Aksela H, Dong C, Heinäsmäki S and Sienkiewicz J 2003 Theoretical Auger and photoionization studies for open-shell atoms and ions *Nucl. Instrum. Methods Phys. Res.* B **205** 93

[26] Fritzsche S 2002 Large-scale accurate structure calculations for open-shell atoms and ions *Phys. Scr.* **T100** 37

[27] Fritzsche S 2001 RATIP—a toolbox for studying the properties of open-shell atoms and ions *J. Electron Spectrosc. Relat. Phenom.* **114** 1155

[28] Fritzsche S, Fricke B and Sepp W-D 1992 Reduced L_1 level width and Coster–Kronig yields by relaxation and continuum interactions in atomic zinc *Phys. Rev.* A **45** 1465

[29] Chen M, Crasemann B, Martensson N and Johannsson B 1985 Residual limitations of theoretical atomic-electron binding energies *Phys. Rev.* A **31** 556

[30] Sairanen O-P, Kivimäki A, Nõmmiste E, Aksela H and Aksela S 1996 High-resolution pre-edge structure in the inner-shell ionization threshold region of rare gases Xe, Kr, and Ar *Phys. Rev.* A **54** 2834

[31] Kikas A, Osborne S, Ausmees A, Svensson S, Sairanen O-P and Aksela S 1996 High-resolution study of the correlation satellites in photoelectron spectra of the rare gases *J. Electron Spectrosc. Relat. Phenom.* **77** 241